ACS APPLIED MATERIALS & INTERFACES

www.acsami.org

Research Article

Morphological and Orientational Controls of Self-Assembly of Gold Nanorods Directed by Evaporative Microflows

Xiaoduo Liu, Ziyu Chen, Qingkun Liu, Ghadah H. Sheetah, Ningfei Sun, Peng Zhao, Yong Xie,* and Ivan I. Smalyukh*

Cite This: *ACS Appl. Mater. Interfaces* 2021, 13, 53143−53154

Read Online

ACCESS | Metrics & More | Article Recommendations | Supporting Information

ABSTRACT: Evaporative self-assembly of noble metal nanoparticles into ordered structures holds great promise for fabricating optical and plasmonic devices by virtue of its low cost, high efficiency, and ease of operation. However, poor control of Marangoni flows is one of the challenges accounting for realizing a well-defined assembly. Herein, based on the theoretical analysis of the influence of evaporative intensity on the assembly, two simple but reliable flow-field-confinement platforms are designed to control the evaporative microflows and to work concurrently with depletion forces to enable the regulated self-assembly of gold nanorods. Orientationally ordered assemblies are realized by the designed strong unidirectional microflow in a capillary, and a device-scale assembly of monolayer membrane is obtained by the created weak convection in homemade glass cells. Morphologically diversified superstructure assemblies, such as spherulite-like, boundary-twisted, chiral spiral assemblies, and merging membranes with a π-twisted domain wall, are obtained due to the spontaneous symmetry breaking or in the presence of defects, such as surface steps and screw dislocations. Optical anisotropy and polarization-dependent behaviors of these assemblies are further revealed, implying the potential applications in plasmonic coupling devices and optoelectronic components. An understanding of the entropy-driven assembly behaviors and control of evaporative microflows to guide the self-assembly of gold nanorods provides insights into the general bottom-up approach that is helpful for constructing complex yet robust nanosuperstructures.

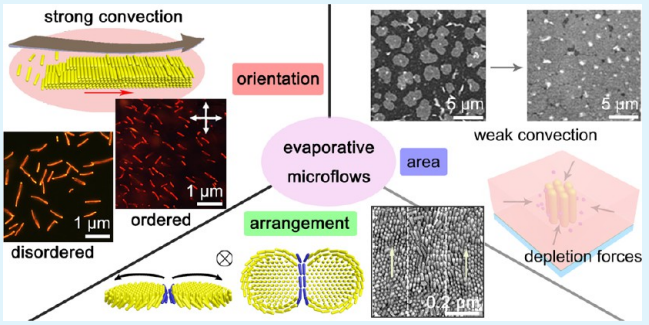

KEYWORDS: *structure regulating, orientationally ordering, large area, self-assemblies, evaporative microflows*

1. INTRODUCTION

Advanced self-assembly techniques have been recently exploited to fabricate hierarchical and sophisticated structures at the micro- or nanoscale for applications in optical/plasmonic devices, optoelectronic sensors, and biomedical imaging devices.[1,2] Evaporative self-assembly, as a nonlithographic approach, has motivated ever-increasing research interest in exploring the ordered structures and their formation mechanisms due to its simple, rapid, and inexpensive virtues.[3−6] However, two problems still significantly limit the evaporative-directed assemblies and their applications. One is that uneven Marangoni flows caused by surface tension gradient during solvent evaporation make the assembly process uncontrollable.[7,8] Another is that only several kinds of simplex assembly structures are realized by the evaporation-induced approaches. Some geometrically symmetrical assemblies with a hexagonal order have been obtained in various systems of CdSe nanorods,[9] PbS nanocrystals,[10] LaF_3 nanoplates,[11] filamentous viruses (*fd*-viruses),[12] etc., but breaking the geometric symmetry of assemblies to obtain shape- and structure-anisotropic superstructures at the nanoscale using highly efficient bottom-up evaporation methods still remains a challenge.

Several strategies have been developed to overcome the difficulties in recent advancements. For example, Alivisatos et al. reported diversified nanocrystal superlattices through a polymer-chain control strategy in which different molecular weights of polystyrene ligands were grafted on the nanocrystals to regulate the assembly superstructures on the surface of an immiscible liquid subphase.[13] In our previous works, by introducing intermolecular J-heteroaggregate interactions between rhodamine 6G molecules, we realized the structural symmetry control of assembled gold nanorod (GNR) superlattices from the minimum-formation-energy hexagonal order to the thermostable tetragonal order.[14] Currently, it has also been predicted that controlled evaporative microflows

Received: July 7, 2021
Accepted: October 19, 2021
Published: October 29, 2021

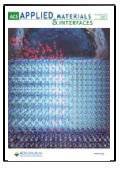

https://doi.org/10.1021/acsami.1c12594
ACS Appl. Mater. Interfaces 2021, 13, 53143−53154

have the capacity to guide the self-assembled superstructures of colloidal nanoparticles.[15,16] For example, Man et al. theoretically analyzed that nanoparticles continuously formed a "coffee ring" structure to volcano-like and mountainlike depositions at the dried droplet periphery, which were ascribed to thermal Marangoni flows driving nanoparticles' transport outward during an evaporation process.[15] Besides, Bhardwaj et al. simulated that through suppressing the "coffee ring" effect, disk deposition can be formed inside the dried droplet.[16] Experimentally, Liu et al. obtained highly ordered layered structures using the superspreading shear flow at an immiscible hydrogel/oil interface.[17] In addition, restricted spaces like two-plate configurations,[18] cylindrical tubes,[19] or "curve-on-flat" geometries have also been used to overcome the uncontrollable Marangoni flows and obtain self-assembled superstructures.[20]

Hence, controllable evaporative microflows can be designed to enable the well-defined self-assembly of nanoparticles. During solvent evaporation, the flow velocity is varied in different regions within the droplet, resulting in imbalanced pressures acting on the assembly according to the Bernoulli principle.[21] Meanwhile, the competition among the influence of evaporative microflows, thermal disturbances, and other interactions (such as depletion, electrostatic, and gravity) will also affect the state of assembly. Herein, the critical flow velocity affecting the self-assembly was first theoretically analyzed to predesign the evaporation condition. The corresponding Peclet number ($P_e = vL/D$, v, evaporative microflow velocity; L, space thickness of glass cells or diameter of the capillary tube; D, diffusion coefficient of molecules in the liquid, $\sim 10^{-9}$ m^2 s^{-1}), an important parameter relying on the velocity of the evaporative microflows, was estimated to further elucidate the key role of convective transfer in the self-assembly of GNRs, which were used as the building blocks.[22] As the P_e is larger than 1, convective transfer plays a major role in the nanorod transportation during the evaporative self-assembly, while as the P_e is smaller than 1, diffusive transfer caused by the concentration gradient of nanorods mainly affects the assembly. The critical evaporation intensity (expressed by flow velocity) that can effectively influence the assembly state was estimated to be about 5.6×10^{-3} m s^{-1}.[21,23] Furthermore, the results of the theoretical analysis show that the flow velocity under strong convection that can orient the assemblies is about 7.5×10^{-3} m s^{-1}. On these bases, experimentally, we developed two simple but efficient flow-field-confinement platforms to control the synergistic interactions between the evaporation microflows and depletion forces for obtaining well-defined regulated self-assemblies of GNRs.[24] Accordingly, orientationally ordered anisotropy assemblies of GNRs were obtained under the designed strong unidirectional convection (flow velocity $> 10^{-3}$ m s^{-1}, $P_e \gg 1$) in a semiopened capillary tube.[25,26] In contrast, an assembled monolayer membrane at the device scale with fewer defects was realized under the created mild convection (flow velocity $< 10^{-5}$ m s^{-1}, $P_e < 1$) in the designed glass cells.[27] Furthermore, morphologically diversified assemblies, such as spherulite-like, boundary-twisted, chiral spiral assemblies, and merging membranes with a π-twisted domain wall, were obtained due to spontaneous symmetry breaking or in the presence of defects, such as surface steps and screw dislocations. Optical anisotropy and polarization-dependent behaviors at the edges of the assemblies were finally revealed by polarized optical microscopy (POM). These findings on evaporative microflows directed well-defined self-assemblies supply a universal, low-cost, and ease-of-operation route for constructing highly ordered superstructures, which would have applications in plasmonic coupling devices, optical/optoelectronic sensors, and biomedical imaging devices.[28−30]

2. EXPERIMENTAL SECTION

2.1. Synthesis of GNRs and Preparation of Assembly Samples. GNRs were synthesized with the aspect ratios ranging from 3.8 to 4.4 by following a well-developed seed-mediated method (Supporting Information, synthesis of GNRs).[31] The as-prepared GNRs were stabilized by the surfactant cetyltrimethylammonium bromide (CTAB, Sigma-Aldrich) in an aqueous dispersion. Specifically, the synthesized GNR solution (~0.5 nM GNRs and ~2.0 mM CTAB, 1 mL) was centrifuged (12 000 rpm, 30 °C for 5 min) and the supernatant was removed. Then, CTAB solution (2.5 mM, 5 μL) was added to the residual solution (~10 μL) and the mixture was dispersed by ultrasonication for about 1 min. The obtained GNR solution (~33 nM GNRs and ~2.2 mM CTAB, 15 μL) was then pipetted into the containers for the following assembly experiments.

2.2. Preparation of the Flow-Field-Confinement Platforms. The sandwich glass cells were prepared by a clean coverslip (0.1 mm in thickness) and a clean glass slide with a small number of silica microspheres as a spacer (5 μm in diameter, from Thermo Fisher Scientific). A layer of curing glue was then applied along the gaps between the edges of two out of four slides to partially seal the cell. Openings on two diametrically opposite sides were reserved for the purpose of filling the assembly solution and guiding the evaporative convection. The capillary tube used has a size of 0.3 mm in diameter and 100 mm in length. One end of the tube was sealed by curing the epoxy glue after injecting the assembly solution into the tube. Unidirectional thermocapillary convection was generated along the longitudinal direction of the tube.

2.3. Conditions for Solvent Evaporation. The intensity of evaporative microflows for controlling the morphology and orientation of self-assembly of GNRs was predesigned based on the theoretical analysis (the details are given in the Supporting Information). The specific evaporation conditions for the experiment were designed referring to the reported works (shown in the Supporting Information) and obtained by adjusting the ambient temperature and relative humidity using a programmable temperature and humidity chamber (STIK, CTHI-150B2).[23,25−27,32] According to our previous work on the influence of environmental temperature on the assembly structure,[33] at a constant humidity of 85%, when the temperature is lower than 25 °C, the crystallization of the surfactant CTAB hinders the assembly of GNRs, while at a higher temperature, the degree of assembly becomes more disordered, which is ascribed to the significant effect of thermal disturbance, and GNRs cannot assemble at a temperature higher than 55 °C. Thus, the ambient temperature was set within an appropriate temperature range of about 25−50 °C and the evaporating microflow velocity was controlled by reducing the relative humidity from 85 to 30% accordingly.

2.4. Control of Self-Assembly of Well-Defined GNRs in the Designed Platforms. Dextran (~10 nm in diameter of globular macromolecules, Aladdin, 50 mg mL^{-1}, 3.5 μL) was added to the prepared GNR solution as an adjustable depletant and homogeneously dispersed by an ultrasonic bath. Then, the assembly solution (15 μL) was pipetted into the designed platforms and filled in the cell space by capillarity. The prepared assembly samples were put into a clean glass Petri dish and placed in a climate chamber. The obtained assemblies were then characterized by optical microscopy (OM, Olympus BX51-P).

For the self-assembly of GNRs under weak convection with the conditions set at a temperature of 25 °C and humidity of 85% (flow velocity: $\sim 10^{-5}$ m s^{-1}),[27,32] the GNR concentration was increased by centrifuging and concentrating the synthesized GNR solution twice and backfilling an appropriate amount of CTAB to ensure that GNRs will not aggregate. (1) To scale up the monolayer assembly area, the

https://doi.org/10.1021/acsami.1c12594
ACS Appl. Mater. Interfaces 2021, 13, 53143−53154

Scheme 1. Schematic of GNR Assemblies with Well-Defined Structures Directed by Evaporative Microflows Using the Developed Platforms[a]

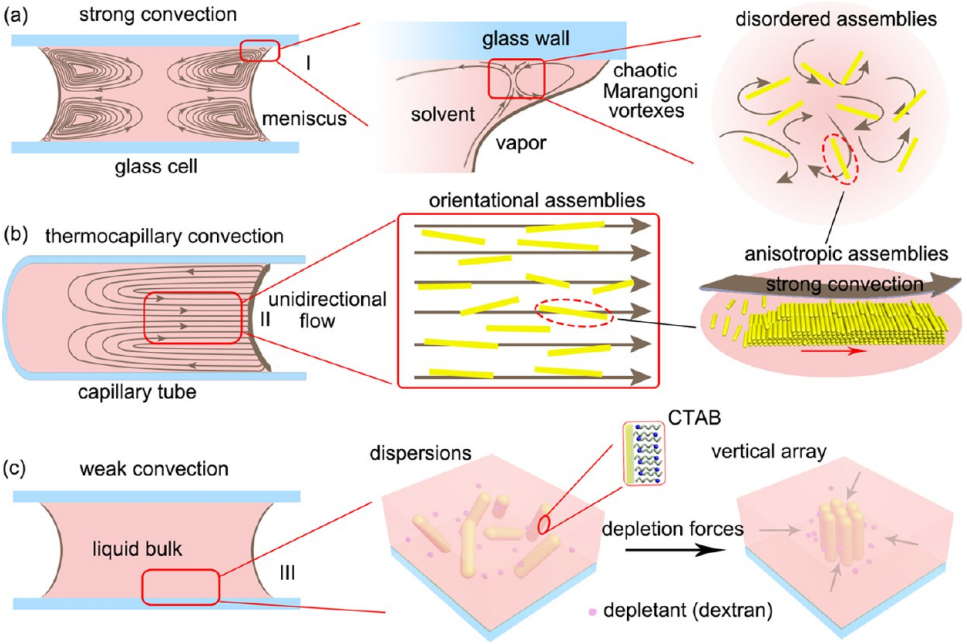

[a](a) Vertically oriented flakelike assemblies with anisotropic shapes directed by strong convection in Region I in the homemade glass cells with a sandwich structure. (b) Orientationally ordered assemblies led by strong unidirectional convection in Region II, near the central area of the capillary tube. (c) Horizontally oriented flakelike assembly with a symmetric geometry driven by depletion forces under weak convection in Region III in the glass cells.

GNR concentration was adjusted (from ~33 to ~70 nM), the assembly time in the climate chamber was set at 30 min, and then the assembly sample was taken out for performing real-time observation of the assembling process under POM. (2) The assembled configurations obtained at a superhigh concentration of GNRs (~0.1 mM) and a longer assembly time of about 1 h were also investigated. (3) During real-time observation, the influence of thermal disturbance on the assembled monolayer membrane was investigated by removing the infrared filter or further heating the assembly sample up to 35 °C using a heating stage (Linkam, THMS600).

For the assembly of GNRs under strong convection (flow velocity > 10^{-3} m s^{-1}), the prepared sample (15 μL, ~33 nM GNRs, ~2.2 mM CTAB, and 3.5 μL of 50 mg mL^{-1} dextran) was used and the evaporation condition was set at a temperature of 40 °C and humidity of 30%.[23,26] To further control the assembly orientation by the designed strong unidirectional convection (flow velocity ~10^{-2} m s^{-1}), the prepared assembly sample containing the same concentration of components was injected into the capillary tube and the evaporative condition was set at a temperature of 50 °C and humidity of 30%.[25] The assembly time of the above samples in the climate chamber was set at 30 min, and then, the samples were taken out for real-time observation of the assembling process under POM.

2.5. Self-Assembly of GNRs by a Droplet Evaporation Method. For the investigation of the assembly geometry and GNR arrangement, the dried assembly samples were further prepared by a droplet evaporation method referring to our previous works on the self-assembly of GNRs.[33,34] Clean silicon wafers (0.7 mm × 0.7 mm) or carbon-supported copper grids (300 mesh, 3.0 mm) were used as substrates for the evaporative experiments. A GNR dispersed droplet (15 μL containing dextran) was dropped onto the substrate, which was placed in a plastic Petri dish with a cover. Then, the Petri dish was placed into a programmable temperature and humidity chamber for controllable evaporation of the droplet at a series of preset humidity and temperature conditions, which are the same as the evaporative conditions for the above-mentioned samples. To ensure that the solvent was evaporated completely, the whole evaporating process of the samples was set to 3.5 h in the chamber. The self-assembled structures were then characterized at some interesting regions within the samples (corresponding to the real-time observed positions within the cells taking into account the similar evaporative conditions) by scanning electron microscopy (SEM) and transmission electron microscopy (TEM).

2.6. Characterization. The spectra of GNRs were collected by an ultraviolet−visible spectrophotometer (UV−vis, Cary50) within 200−1100 nm at a scan rate of 600 nm min^{-1}. A quartz colorimetric-ware (1 cm × 1 cm) was used for spectrum collection. The zeta (ζ) potential of the GNR solution with dextran (50 mg mL^{-1}) or without dextran was examined by a Zetasizer Nano ZS290 Instrument. The dispersant was water, the temperature was set at 25 °C, and the cell type was a clear disposable zeta cell. Measurements for one sample were performed three times, and an average value was used as the final result. The optical images of the assemblies were captured by an OM with a heating stage using 100× and 50× oil immersion objectives. For polarized images of these kinds of liquid crystal-like states, a phase retardation plate (λ = 530 nm, Olympus) was used to analyze the optical anisotropy of samples. For dark-field imaging, an oil immersion dark-field condenser with a numerical aperture of 0.9 (U-DCW, Olympus) was used. SEM images were acquired using a Hitachi S-4800 microscope operating at 10 kV for secondary electron imaging. The assembled geometry of GNRs was determined both from the SEM images and their fast Fourier transform (FFT) pattern. TEM images were acquired with a JEM-2100 microscope operating at an accelerating voltage of 200 kV.

3. RESULTS AND DISCUSSION

3.1. Design of Structure-Regulated Evaporative Self-Assembly of GNRs. To better realize the evaporative microflow-directed self-assembly, a simple theoretical analysis was first conducted (the details are shown in the Supporting Information) to determine the role of evaporative microflows (expressed by flow velocity) in directing self-assembly. The

https://doi.org/10.1021/acsami.1c12594
ACS Appl. Mater. Interfaces 2021, 13, 53143−53154

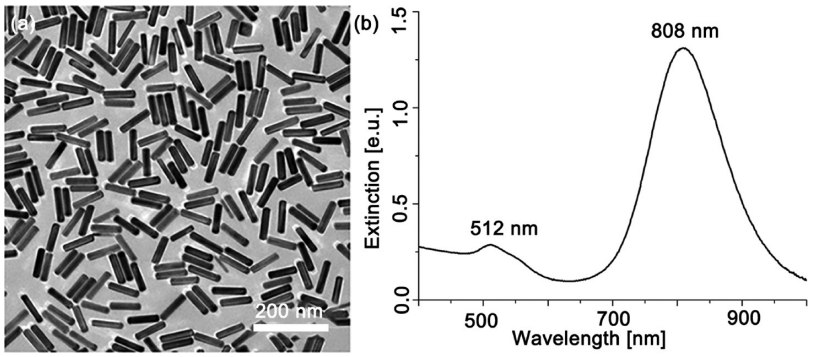

Figure 1. Morphological and spectroscopic characterization of the synthesized GNRs. (a) SEM image showing the morphologies and size monodispersity of GNRs with an aspect ratio of about 4. (b) UV−vis absorption spectrum of the GNR dispersion showing a narrow surface plasma resonance (SPR) absorption peak at 808 nm.

theoretical analyses were based on the energy competitions among thermal disturbance, evaporative microflows, and gravitational potential energy of the assembly during solvent evaporation.[21] The relevant Peclet numbers (P_e) were estimated to further elucidate the effect of evaporative convection on the self-assembly.[22] In general, colloidal nanorods first form assembly nuclei in solution and assemble into small lamella with a symmetrical structure driven by the depletion forces. The assembly states of the lamella are mainly affected by the evaporative microflow-induced pressure, their own gravity, and thermal disturbance. Specifically, the flow velocity is continuously varied in the vertical direction within the evaporating solution (the closer to the substrate, the slower the velocity).[23] According to the Bernoulli equation[21]

$$p + \rho g h + \frac{1}{2}\rho v^2 = c$$

(where p is the pressure, ρ is the density of pure water, h is the height, v is the flow velocity, and c is a constant) evaporative microflows can lead to a pressure difference on the upper and lower surfaces of the lamella. As the force generated from the pressures (expressed by F_1 and F_2) can overcome the assembly's gravity ($G_{assembly}$), i.e., $F_1 - F_2 > G_{assembly}$, the evaporative microflows can make the assembly move upward in the evaporating solution. The critical flow velocity ($\overline{v}$) is accordingly calculated to be about 5.6×10^{-3} m s^{-1}. The corresponding P_e is about 28, higher than 1, meaning that the evaporative convection should play a major role in the formation of the assembly. While the small gravity of the lamella in this situation still cannot overcome the influence of thermal disturbance, i.e., $G_{assembly} < k_BT$, this would result in imbalanced forces and cause the assembly easy to flip and spontaneously orientate vertically in solution, as illustrated in Scheme S1a−f. The critical assembly size (l_0) is thus estimated to be about 3 μm. This result suggests that during the initial assembly period, the influence of thermal disturbance cannot be neglected. To better represent the changes caused by these influences, a velocity vector analysis diagram is obtained, as shown in Scheme S1i (including the effects of flow vector, thermal disturbance, and assembly orientation), suggesting that only as the evaporative flow velocity (v_{flow}) is larger than 7.5×10^{-3} m s^{-1} with P_e of about 10^3, the influence of convection ($W_{flow} \approx 20k_BT$) just right suppresses the thermal disturbance and orientates the assembly along the directions of the flow field.

According to the above theoretical analysis results, we designed the following flow-field-confinement platforms as illustrated in Scheme 1, in the forms of homemade glass cells and a capillary tube, to realize the morphological and orientational controls of self-assembly of GNRs. The surface property of the designed platforms was characterized first by measuring the contact angle of water on the substrate, as shown in Figure S1 (Supporting Information). The contact angle was 37° for the glass slide and 49° for the capillary tube, suggesting that the surfaces of the designed platforms are both hydrophilic. Such substrates are prone to prevent the droplet from quickly shrinking based on the reports of Hu et al. and our previous work,[33,35] which are conducive to the formation of the self-assembly of GNRs.

GNRs with a bilayer of cetyltrimethylammonium bromide (CTAB) and a uniform aspect ratio of about 4 (length, 81 ± 2 nm; diameter, 19 ± 2 nm) (Figure 1a), easy to form self-assembly demonstrated by our previous work,[33] were used as the building blocks.[31] The UV−vis absorption spectrum of the GNR dispersion (Figure 1b) shows a narrow surface plasma resonance (SPR) peak at about 808 nm, suggesting a narrow size distribution of GNRs.[36,37] In the GNR solution, a nonadsorbed polymer, dextran, was introduced as the depletant to enhance the entropic depletion forces (also arising due to the micelles of CTAB molecules self-assembling within the solution) to drive the self-assembly.[38,39] The ζ-potential of the GNR solution with or without dextran was examined, as shown in Figure S2, indicating that the surface potential of GNRs is around 55 mV and increases with an increase of CTAB concentration. Also, the potential of the GNR solution with dextran shows no significant change compared with that of the GNR solution without dextran, implying that the macromolecule polymer, dextran, cannot interact with CTAB owing to its electrical stability in aqueous solutions.

For the solvent evaporating in the glass cells, the changes in surface tension caused by the temperature and solute concentration gradients bring about evaporative convection and the convection intensity usually weakens from the meniscus interfaces (between the solvent and vapor) to the liquid bulk (Scheme 1a).[40] In our experimental design, the resulting strong convection (flow velocity > 10^{-3} m s^{-1}, $P_e > 1$) near the three-phase contact lines (defined as Region I) can constrain GNRs to assemble into shape-anisotropic structures with the anisotropic axes parallel to the direction of the convection (Scheme 1b).[23] In contrast, the weak convection

https://doi.org/10.1021/acsami.1c12594
ACS Appl. Mater. Interfaces 2021, 13, 53143−53154

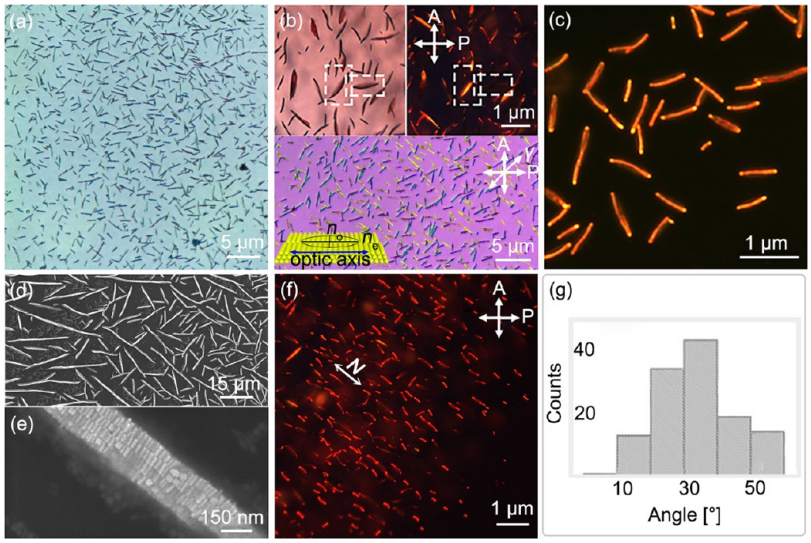

Figure 2. Vertically oriented edge-on flakelike assemblies with anisotropic geometries assisted by strong convection. (a) Randomly distributed assemblies observed under OM. (b) Birefringence of the assemblies under OM (top-left) and POM (top-right). The bottom image was taken under POM with an inserted phase retarder having the slow axis γ placed at 45°. (c) Dark-field image showing the scattering light of the assemblies. (d, e) SEM images showing the highly anisotropic shape of the assemblies and the corresponding nanoarrangement of GNRs. (f) POM image of the orientationally ordered assemblies obtained by the designed unidirectional convection within the capillary tube. The capillary tube was placed at 31.5° with respect to the polarizer direction ***P*** during imaging. The vector ***N*** in (f) indicates the average orientational direction of the assemblies. (g) Orientational distribution diagram of the assemblies.

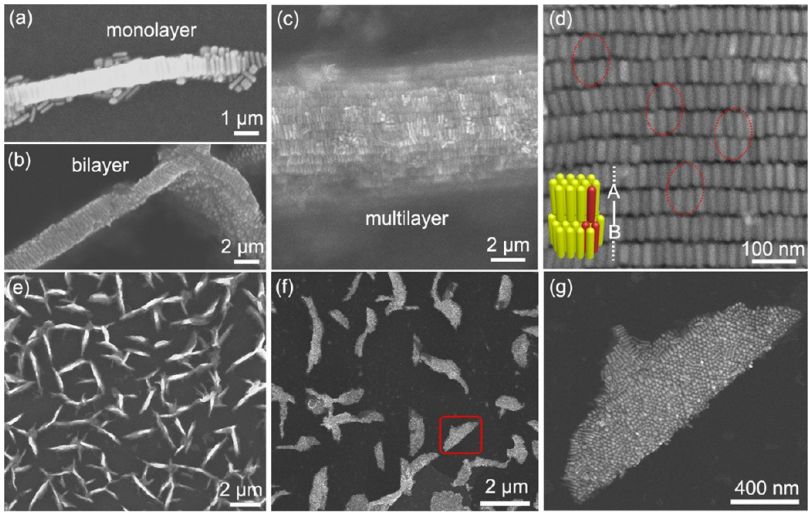

Figure 3. SEM images showing the edge-on flakelike assemblies. (a) Assembled monolayer with the nanorods aligning side by side and parallel to the substrate. (b) Bilayer with a similar nanostructure. (c) Corresponding multilayer nanostructure. (d) Enlarged SEM image showing the interlaced A−B alignment as marked by the red circles. The inset shows the three-dimensional schematic with a hexagonal superlattice. (e) Obliquely oriented flakelike assemblies on the substrate. (f) Horizontally oriented flakelike assemblies showing the anisotropic shapes of the assemblies, obtained in the last stage of the droplet evaporation with the receding liquid level. (g) Enlarged assembly flake in (f) showing the hexagonal vertical array of GNRs and its sharp edge, suggesting substrate-confined growth in the solution.

(flow velocity < 10^{-5} m s^{-1}, P_e < 1) appearing away from the meniscus (defined as Region III) can prevent the coffee ring effect and promote the assembled monolayers. In this circumstance, the formation of the assembly mainly depends on the concentration of GNRs. According to the theoretical simulation of Bhardwaj et al.,[16] in this condition, depletion forces can lead GNRs to assemble into isotropic arrays along the surface of the substrate (Scheme 1c).[16,27,37] For the solvent evaporating in the capillary tube, the surface tension caused by the nonuniform temperature gradient induces thermocapillary convection near the meniscus interfaces (Scheme 1b).[41−43] Two symmetric vortices form in the longitudinal section of the tube and a unidirectional flow hence appears parallel to the axial direction of the capillary tube (defined as Region II).[43] This strong unidirectional convection (flow velocity of about 10^{-2} m s^{-1}, $P_e \gg 1$) can be used to guide the orientation of the assemblies.[25,26] Based on the designed flow field, we have obtained the following well-defined self-assemblies of GNRs.

3.2. Anisotropic Assembled Superstructures Induced by Strong Convection. Numerous disordered anisotropic assemblies of GNRs were first obtained under the strong convection in Region I within the glass cells, as shown in Figure 2a. The velocity of evaporative microflows (more than 10^{-3} m s^{-1}, P_e > 1) and the shear rate are higher near the

https://doi.org/10.1021/acsami.1c12594
ACS Appl. Mater. Interfaces 2021, 13, 53143−53154

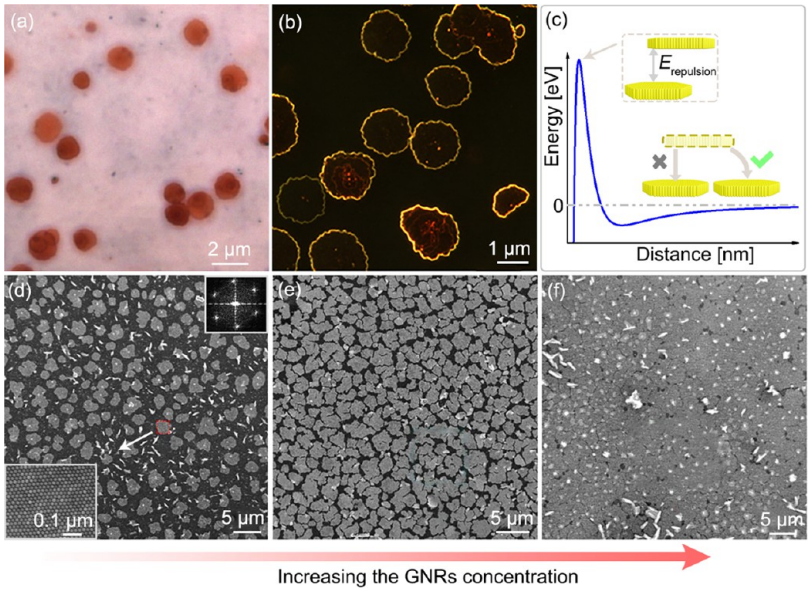

Figure 4. Horizontally oriented assembly membranes under weak convection. (a) OM image showing the obtained assembly membranes. (b) Dark-field image showing the edge scattering states of the assembly. (c) Formation cause of the observed preferential monolayer. The schematic curve shows the variation of potential energy with distance, detailed calculations referred to our previous work,[33] indicating that the larger potential barrier hinders the assembly into a multilayer structure. The inset schematics show such a formation process. (d–f) SEM images showing the variation of assembly area with an increase of GNR concentration. A device-scale assembly membrane was finally obtained as shown in (f). The bottom inset in (d) shows the arrangement of the nanorods in the membranes, and the top inset is the corresponding FFT showing a hexagonal close-packed symmetry of the assembly.

meniscus than those within the liquid bulk, which plays a main role in affecting the orientations of these assemblies and their anisotropic shapes.[44] Additionally, the relative concentration of GNRs is the highest in this region, also influencing the formation of colloidal superstructures due to the depletion forces. Also, for the assembly with a smaller size (<3 μm), thermal disturbance can lead to disordered orientations of these assemblies. The optical micrographs revealing birefringence of the assemblies (along with linear dichroism), composed of bright and extinct dark domains, were obtained using crossed polarizers (oriented along the image edges), as shown in Figure 2b (top images). When a phase retarder with its slow axis marked by γ was added, blue of the second order of interference appeared in the assemblies with the anisotropic axes (i.e., long axes of the assemblies) along 45° and correspondingly yellow of the first order of interference emerged within the assemblies orientating along 135° (Figure 2b, bottom image). We noted that the colloidal self-assemblies had optical behavior resembling that of a positive-anisotropy crystal with the extraordinary n_e and ordinary n_o refractive indices such that $n_e > n_o$. Therefore, the slow axis of the assembly should be the anisotropic axis of the assembly, as shown in Figure 2b, schematic inset. These observations are consistent with the fact that CTAB surfactant molecules within the self-assemblies are oriented perpendicular to GNRs and contribute to the linear birefringence of the overall colloidal superstructures. Under the dark-field mode of microscopy, uniform and intense scattering light appeared, as shown in Figure 2c, reflecting the edge-enhanced optical response of the assemblies. SEM images further reveal the vertically oriented edge-on configuration with an anisotropic geometry (Figure 2d) and an ordered arrangement of the nanorods with a side-by-side mode (Figures 2e and 3a–d), confirming that the rods align each with their long axis perpendicular to the anisotropic axis of the assembly. In addition, monolayer (Figure 3a), bilayer (Figure 3b), and multilayer (Figure 3c) assemblies are further revealed, showing the broad structural variation of these assemblies. The formation of the multilayer structure of these perpendicular assemblies is ascribed to the strong convective transfer of nanorods in the solution, which makes the nanorods assemble both along the transverse and longitudinal directions of the "edge-on" assembly and form a multilayer structure, as shown in Scheme 1b (right schematic). The enlarged SEM image in Figure 3d further shows the interlaced A–B stacking model of the nanorods (Figure 3d, inset) between the neighboring assembly layers, which is attributed to the closest packing having the minimum formation energy (Scheme 1b).

The formation of these assemblies implies the growth process that GNRs form first the assembly nucleus and then grow into the isotropic structure in the initial stage (Scheme S1a), and the increased own gravity of the assemblies overcomes thermal disturbance and causes them to deposit on the substrate. Meanwhile, affected by the constraint of the flow field under strong convection, the assemblies further grow into the anisotropic flakelike structures, as shown in Figures 2a and 3e; also, the small-size assemblies present random distribution owing to the unfavorable effect of thermal disturbance. The observed assemblies always have a sharp flat side (Figure 3f,g) resulting from the substrate-confined growth.

3.3. Orientational Control of the Assembly. To suppress the unfavorable effect of random evaporative microflows and thermal disturbance during the initial assembly period, we designed a capillary tube with its one end open to induce strong unidirectional thermocapillary convection (flow velocity $\sim 10^{-2}$ m s^{-1}, $P_e \gg 1$) and control the orientation of the assembly (Region II in Scheme 1b).[23] Orientationally ordered assemblies were obtained as shown in Figure 2f. The

https://doi.org/10.1021/acsami.1c12594
ACS Appl. Mater. Interfaces 2021, 13, 53143–53154

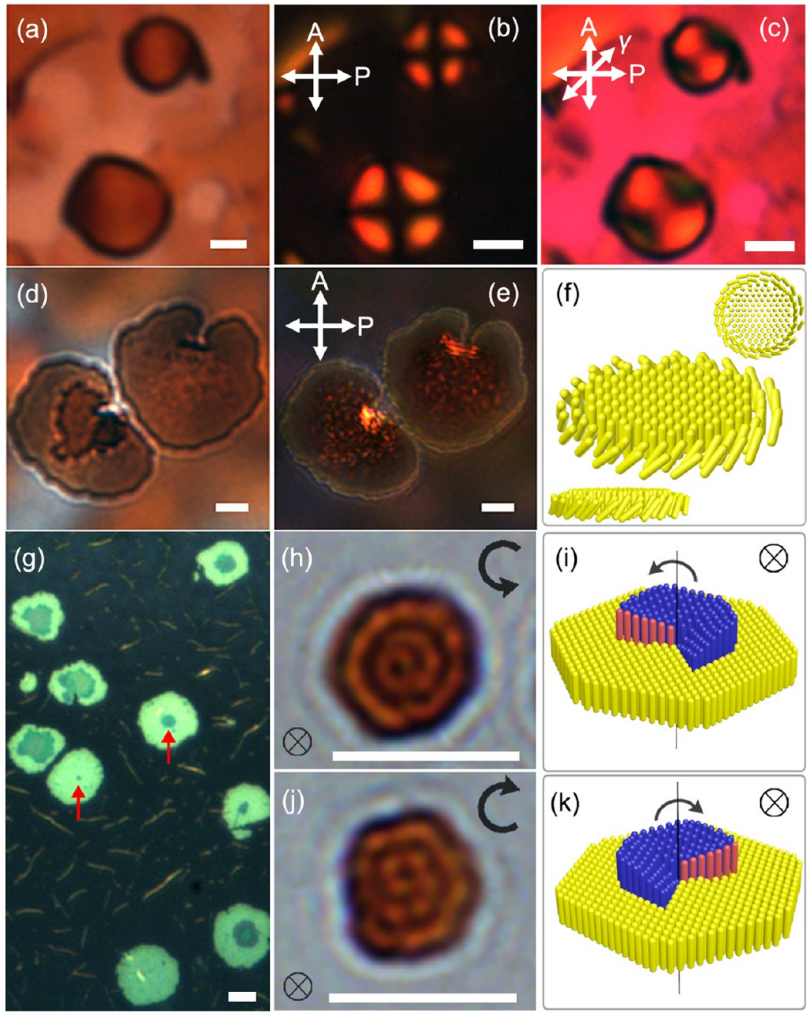

Figure 5. Diversified complex fine textures within the assemblies imaged under OM. (a–c) Spherulite-like assemblies, obtained under a high concentration of GNRs and a long assembling time. (d–f) Edge-twisted chiral assemblies, obtained under slight convective disturbance. The schematic diagrams in (f) show the edge-twisted arrangements of GNRs from different perspectives. (g) Multilayer assemblies induced by surface steps. (h, j) Two kinds of spiral multilayer assemblies with distinguishable handedness for left-handedness (h) and right-handedness (j). (i) and (k) Corresponding schematic diagrams of (h) and (j), respectively, showing the formation of the spiral multilayers induced by screw dislocations. The curved arrows indicate the handedness of the assembly. The scale bars are 0.5 μm.

two-dimensional (2D) scalar order parameter of the assemblies was estimated to be about 0.9 by the following equation[38,39]

$$S_{2D} = 2\langle \cos^2 \theta \rangle - 1$$

where θ is the angle between the anisotropic axis of the assembly and the average orientational direction $\boldsymbol{N}$. The statistical orientational distribution (relative to the polarizer direction $\boldsymbol{P}$) (Figure 2g) indicates that the assembly direction $\boldsymbol{N}$ is along the capillary axis due to the effect of the unidirectional convection. With an increase of assembling time and particle concentration near the meniscus interfaces, the assemblies vary from the vertically oriented edge-on flakes to the obliquely oriented ones (Figure S3) due to an increase in the assembly area. Although the shape anisotropy of the assemblies becomes slightly degenerated over a long period, their orientations keep being ordered. These results verify that the strong microflows can not only direct the orientations of the self-assemblies with shape anisotropy but also facilitate their growth in a controllable direction.

3.4. Transitional Variation of the Assembly with Decreasing Convective Intensity. We also investigated the assemblies formed in the different regions within the confined space, as shown in Figures S4 and S5. We found that the shape anisotropy of the assembly became unremarkable when the convective intensity was weakened. Specifically, the strong convection both near the three-phase lines in the cell and near the vapor–liquid interfaces in the tube can constrain the nanorods to assemble along one preferential growth direction, consistent with the convection direction, and then assemble into the anisotropic flakelike assemblies with a vertical orientation to the substrate (Figure 2). As the concentration of nanorods increased near the three-phase contact lines, GNRs gradually assembled into the oblique or bent flakes, as shown in Figures 3e and S4. In the region slightly away from the vapor–liquid interfaces in the cell, as illustrated in Scheme 1c, the convective intensity became trivial (flow velocity < 10^{-4} m s^{-1}) and a small number of horizontally oriented assembly membranes with symmetric geometries appeared while the vertically oriented flakes faded away gradually (Figure S5). As the solution environment was close to a quasi-static situation (flow velocity ~10^{-5} m s^{-1}), the assembly membranes dominated (Figure 4).

https://doi.org/10.1021/acsami.1c12594
ACS Appl. Mater. Interfaces 2021, 13, 53143–53154

3.5. Scaling-Up of the Area of Monolayer Assembly. To control and scale up the assembly membranes, we created a mild evaporative condition with the flow velocity < 10^{-5} m s^{-1} to suppress the coffee ring effect on the assembly, as shown in Figure 4.[27] In such a case, many horizontally oriented assembly islands with an average assembly area of about 2 μm^2 were first obtained (Figure 4a). Under the dark-field mode of OM (Figure 4b), strong edge scattering states show a corrugated contour of these assemblies. Through real-time observation under OM in Figure S6a, a linear growth rate of 0.8 nm/s in diameter (Figure S6b) is revealed, implying a stable and orderly growth process. The arrangement of nanorods within the assemblies is further uncovered by SEM imaging (Figure 4d), illustrating that the nanorods align into horizontally monolayer assembly with a vertical orientation of their long axes and a perfect hexagonal close-packed array (Figure 4d, insets). The prominent monolayer is attributed to the relatively large electrostatic barrier, arising from a large quantity of positive charges of CTAB molecules adsorbed on the surface of the assembled membranes, suppressing the formation of multilayered structures,[34,44] as shown in Figure 4c. Notably, device-scale self-assembled membranes with a scale of 1 cm or more were finally obtained by successively increasing the concentration of GNRs in the solution, as presented in Figure 4d–f, suggesting the possibility of preparation of monolithic membranes with features of high ordering, large area, and single-nanorod thickness.

3.6. Diversity in the Assembly Configurations. Besides the control on the orientation, anisotropic shape, and area of the GNR assembly, under the weak convective conditions, diversified ordered configurations were also obtained based on the spontaneous symmetry breaking or in the presence of defects. (i) A spherulite-like assembly presented in Figures 5a–c and S7, under OM, POM, and POM with the phase retarder, was obtained because of the spontaneous symmetry breaking under the conditions of a higher GNR concentration (~0.1 mM) and a long assembly time (~1 h). A Maltese crosslike texture, similar to the textures known for liquid crystal (LC) droplets,[45] is shown in Figures 5b and S7b–d. With the help of the phase retarder, the director distribution is identified in Figures 5c and S7e,f, with the interference colors suggesting that the director has a radial distribution where GNRs tilt from the periphery toward a central point. The formation is related to the high particle volume fraction during the evaporative self-assembly process. According to the reports of Frenkel et al. and Lekkerkerker et al., the superhigh concentration of GNRs can first form a metastable dense fluid state with a reduced free-energy barrier for assembly nucleation.[45,46] With the solvent evaporating, the nanorod concentration becomes higher, which can make the size of the dense fluid expand, while the GNRs arrange spontaneously into a three-dimensional spherulite-like radial configuration, as schematically illustrated in Figure S7a.[46,47] (ii) Another two kinds of ordered configurations, chiral self-assemblies, as shown in Figure 5d–k, were obtained by applying additional thermal fluctuations on the assembled monolayer membrane. After a moderate assembly period of about 30 min, the assembly sample was taken out of the climate chamber and observed under OM. One of the processing methods was removing the infrared filter of the OM to generate a slight thermal disturbance on the assembled sample. This disturbance led to a twisted orientation of the nanorods at the edges of the monolayer membrane and formed the edge-twisted self-assemblies, as shown in Figure 5d,e. Its birefringence arises mainly at the periphery of the assembly and distributes evenly, suggesting a slight twist of the component nanorods in this area. The central part of the assembly is dark, which reflects the different alignments of GNRs (Figure S8). It is considered that the twist of nanorods should emerge at the edge and be expelled from the bulk, as shown in Figure 5f schematics.[48] The peripheral nanorods are thought to have an equal chance to twist along a left-handed direction or a right-handed direction (Figure S8c,d), resulting in symmetry breaking that accompanies entropy maximization.[49,50] The TEM image in Figure 6 confirms these twisted

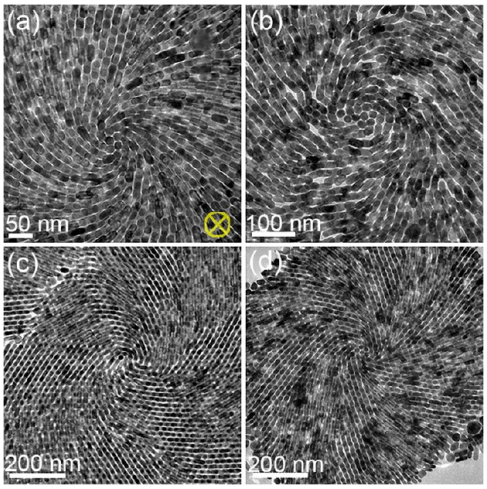

Figure 6. TEM images showing the nanoarrangements of the twisted self-assembly in a dried state. Twisted GNR assemblies either have features of right-handedness (a and b) or left-handedness (c and d).

superstructures. The twisted degree of the orientation of nanorods in the dried assembled sample becomes more prominent. The center of the assembly consists of vertically aligned nanorods, while the rest of the assembly seems to be composed of horizontal nanorods. According to our previous work,[51] when the solvent has been largely evaporated, the dynamic vortex microflows form in the thin solvent layer. The resulting Stokes drag force would drag the substable nanorods along the direction of microflows. As the solvent is completely evaporated, the force leads GNRs to eventually assemble into the twisted self-assemblies with vortical configurations. (iii) Another processing method was to deliberately heat the assembled sample up to 35 °C using the heating stage; the chiral multilayer assemblies, as shown in Figure 5g–k, were obtained under the effect of turbulent convection. The convection leads to a small number of topological defects, such as surface steps and screw dislocations, appearing on the surface of the membrane. These defects sites with lower formation energy promote the nanorods to assemble helically into chiral multilayer structures.[52,53] Figure 5g shows such kinds of chiral multilayer assemblies caused by surface steps, and Figure 5h,j shows the chiral multilayer structures caused by screw dislocations. The handedness of these assemblies appears to be tunable relying on the formation ways of the screw dislocations, as shown in Figure 5i for left-handedness and Figure 5k for right-handedness.[52] Because of the special optical anisotropy of these chiral self-assemblies, they have potential applications in optical sensors and chiral plasmonics.[53]

https://doi.org/10.1021/acsami.1c12594
ACS Appl. Mater. Interfaces 2021, 13, 53143–53154

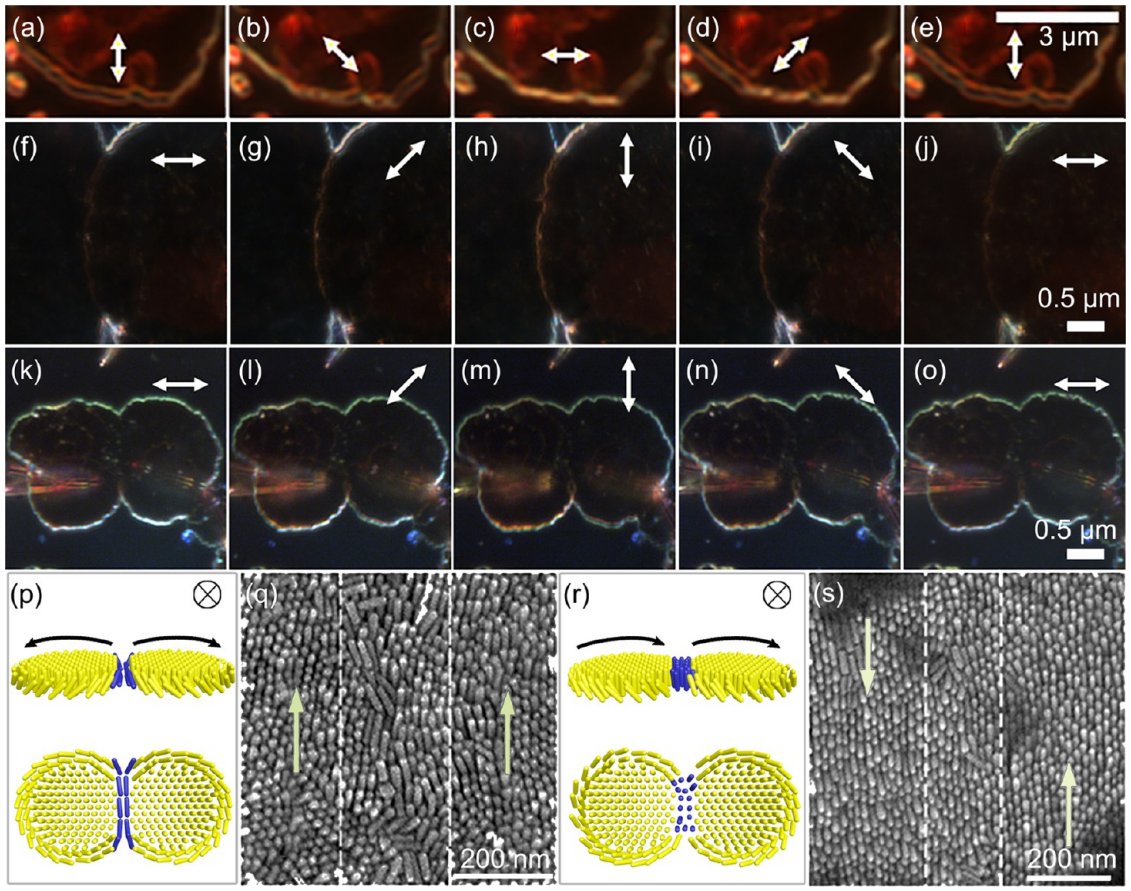

Figure 7. Polarization-dependent effects at the edges of the assemblies. (a–e) Polarized dark-field micrographs of a single assembly island. (f–j) Polarized light characterization of two merging assemblies with a distinguishable π-twisted domain wall in the merging area. (k–o) Polarized response of two merging assemblies without the observable domain wall. The white double arrows in (a–o) represent the orientation of the polarizer. (p) and (r) Schematic diagrams of the formation of the π-twisted domain wall in the merging area between two twisted assembly membranes with inverse or identical handedness of the twist at the periphery of domains. The blue rods illustrate the detailed arrangements of GNRs within the merging areas. (q) and (s) SEM images showing the arrangements of GNRs near the domain walls. The arrows in (q) and (s) represent GNRs tilted within the twisted regions of islandlike assemblies that are merging.

3.7. Merging Interplays between Two Assembled Membranes. Considering the edge-twisted states of the assemblies and the resulting optical anisotropy, the polarization-dependent behaviors at the boundaries of the assembled membrane were further investigated using the dark-field mode of OM, as shown in Figure 7a–e. The polarizer was parallel to the assembly plane, and its polarized direction was along the edge of the field of view. As the direction of polarization changes, the strongest scattering occurred at the position that the orientation of the polarizer was parallel to the boundary of the assembly (Figure 7c), while the scattering was the weakest when the polarizer was oriented orthogonally to the boundary of the assembly (Figure 7a,e). This phenomenon is consistent with our former judgment about the twisted orientation of nanorods along the edges.

Furthermore, we investigated the common merging interplays between two edge-twisted assemblies with opposite or identical handedness. Dark-field microscopy with an oil immersion was adopted to detect the slight variation of the scattering light in the merging area of the two contacting assemblies, as shown in Figure 7f–o. For two assemblies with opposite handedness (Figure 7f–j), a weak scattering signal was observed at the merging area when the polarizer was placed in the vertical direction of the field of view, as shown in Figure 7h. As the polarizer was turned to the horizontal direction, this signal was extinct (Figure 7f,j). This phenomenon is because the opposite handedness of the two assemblies can lead to an almost 90° twist of the rods within the merging area, similar to that in the nematic phase of LCs.[54,55] A schematic in Figure 7p shows the formation of this kind of merging assemblies with the π-twisted domain wall where the rods in the merging area turn to the horizontal alignment due to the constraint on orientation within the merging domains.[55] In contrast, no such π-twisted domain wall was found in the merging area when two assemblies merged with identical handedness at their peripheries, as shown in Figure 7k–o. SEM images in Figure 7q,s further reveal the details of the merging assemblies of GNRs, showing that depending on the handedness of the assembly membranes, the merged island assemblies form either with π-twisted domain walls or without such walls (Figure 7r). Our observations echo similar wall structures to those found in LCs,[54,55] magnetic thin films,[56] and assembled membranes of viruses.[57]

4. CONCLUSIONS

In summary, we have achieved the regulations on well-defined self-assemblies of GNRs by controlling evaporative microflows, synergetically utilized along with entropy-driven depletion

https://doi.org/10.1021/acsami.1c12594
ACS Appl. Mater. Interfaces 2021, 13, 53143–53154

forces. We have also theoretically analyzed the influence of evaporative microflows on the assembly that strong convection can affect the morphology and orientation of the self-assembly. Based on this, we developed simple but reliable flow-field-control platforms providing effective strategies to obtain the well-defined assembly superstructures, which are inaccessible to depletion forces alone. By adjusting the synergistic action between evaporation microflows and depletion forces, the assembly orientation, area, and configuration were regulated. Specifically, strong convection can make colloidal GNRs assemble into vertically oriented structures, such as the edge-on flakelike assemblies in our experiments. By imposing the strong unidirectional convection, it can control the orientation of the assemblies and obtain the overall orientationally ordered liquid crystalline superstructures. In contrast, by creating the weak convection it can regulate GNRs assemble into large-area, defect-free, and monolayer membranes with potential device applications. Moreover, under weak convection, diversified assembly configurations, such as spherulite-like, edge-twisted, and defect-induced, can be further obtained in the presence of spontaneous symmetry breaking or defects. Investigating the merging interplays between two contacting assembly membranes, the π-twisted domain wall was further found. Our research advances control of the entropy-driven self-assembly of noble metal nanoparticles and supplies a generalized way to promote the bottom-up superstructure preparation technique with low cost, ease of operation, and scalable merits.

■ ASSOCIATED CONTENT

Supporting Information

The Supporting Information is available free of charge at https://pubs.acs.org/doi/10.1021/acsami.1c12594.

Experiment details of the synthesis of GNRs, theoretical analysis of the influence of evaporative microflows on self-assembly, tests of the hydrophilic and hydrophobic properties of the used substrates, ζ potential of GNR solution with or without dextran, OM and SEM images of the anisotropic assembly, OM images of the coexisted intermediate state, dynamic growth rule of the assembled membrane, OM images of the spherulite-like self-assembly, OM images of the edge-twisted self-assembly, and supplementary references (PDF)

■ AUTHOR INFORMATION

Corresponding Authors

Yong Xie − *School of Physics, Beihang University, Beijing 100191, China; Key Laboratory of Intelligent Systems and Equipment Electromagnetic Environment Effect, School of Electronic and Information Engineering, Beihang University, Beijing 100191, China;* orcid.org/0000-0003-3574-2883; Email: xiey@buaa.edu.cn

Ivan I. Smalyukh − *Department of Physics, Material Science and Engineering Program, Department of Electrical, Computer, & Energy Engineering, and Liquid Crystal Materials Research Center, University of Colorado, Boulder, Colorado 80309, United States; Renewable and Sustainable Energy Institute, National Renewable Energy Laboratory and University of Colorado, Boulder, Colorado 80309, United States;* orcid.org/0000-0003-3444-1966; Email: ivan.smalyukh@colorado.edu

Authors

Xiaoduo Liu − *School of Physics, Beihang University, Beijing 100191, China*

Ziyu Chen − *School of Physics, Beihang University, Beijing 100191, China*

Qingkun Liu − *Department of Physics, Material Science and Engineering Program, Department of Electrical, Computer, & Energy Engineering, and Liquid Crystal Materials Research Center, University of Colorado, Boulder, Colorado 80309, United States; Department of Physics, Cornell University, Ithaca, New York 14850, United States*

Ghadah H. Sheetah − *Physics Department, College of Science, King Faisal University, Hofuf 31982, Saudi Arabia*

Ningfei Sun − *School of Physics, Beihang University, Beijing 100191, China*

Peng Zhao − *School of Physics, Beihang University, Beijing 100191, China*

Complete contact information is available at: https://pubs.acs.org/10.1021/acsami.1c12594

Author Contributions

Y.X. and I.I.S. conceived the idea. X.L., Q.L., and Y.X. performed the most experiments, analyzed the results, and wrote the draft. Y.X. and I.I.S. guided the project, discussed, and revised the manuscript. G.H.S. supplied the GNR solution and related characterization. The manuscript was written through the contribution of all authors. All authors have given approval to the final version of the manuscript.

Notes

The authors declare no competing financial interest.

■ ACKNOWLEDGMENTS

This work was supported by the Fundamental Research Funds for the Central Universities, the Natural Science Foundation of Beijing, China (No. 2202026), and the National Natural Science Foundation of China (No. 11774018). This research was partially supported by the U.S. National Science Foundation through grant DMR-1810513 (Q.L., G.H.S., and I.I.S.). The authors are thankful to the Analysis and Testing Center of the Beihang University and the Liquid Crystal Materials Research Center of the University of Colorado (Boulder) for their support in the characterization.

■ REFERENCES

(1) Wei, W.; Bai, F.; Fan, H. Y. Oriented Gold Nanorod Arrays: Self-Assembly and Optoelectronic Applications. *Angew. Chem. Int. Ed.* **2019**, *58*, 11956−11966.

(2) Scarabelli, L.; Coronado-Puchau, M.; Giner-Casares, J. J.; Langer, J.; Liz-Marzán, L. M. Monodisperse Gold Nanotriangles: Size Control, Large-Scale Self-Assembly, and Performance in Surface-Enhanced Raman Scattering. *ACS Nano* **2014**, *8*, 5833−5842.

(3) Deng, K.; Luo, Z. S.; Tan, L.; Quan, Z. W. Self-Assembly of Anisotropic Nanoparticles into Functional Superstructures. *Chem. Soc. Rev.* **2020**, *49*, 6002−6038.

(4) Lai, G. H.; Butler, J. C.; Zribi, O. V.; Smalyukh, I. I.; Angelini, T. E.; Purdy, K. R.; Golestanian, R.; Wong, G. C. L. Self-Organized Gels in DNA/F-Actin Mixtures without Crosslinkers: Networks of Induced Nematic Domains with Tunable Density. *Phys. Rev. Lett.* **2008**, *101*, No. 218303.

(5) Li, P. H.; Li, Y.; Zhou, Z. K.; Tang, S. Y.; Yu, X. F.; Xiao, S.; Wu, Z. Z.; Xiao, Q. L.; Zhao, Y. T.; Wang, H. Y.; Chu, P. K. Evaporative Self-Assembly of Gold Nanorods into Macroscopic 3D Plasmonic Superlattice Arrays. *Adv. Mater.* **2016**, *28*, 2511−2517.

(6) Wei, W. B.; Wang, Y. R.; Ji, J. J.; Zuo, S. S.; Li, W. T.; Bai, F.; Fan, H. Y. Fabrication of Large-Area of Vertically Aligned Gold Nanorods. *Nano Lett.* **2018**, *18*, 4467−4472.
(7) Han, W.; Lin, Z. Q. Learning from "Coffee Rings": Ordered Structures Enabled by Controlled Evaporative Self-Assembly. *Angew. Chem. Int. Ed.* **2012**, *51*, 1534−1546.
(8) Rosu, C.; Chu, P. H.; Tassone, C. J.; Park, K.; Balding, P. L.; Park, J. O.; Srinivasarao, M.; Reichmanis, E. Polypeptide Composite Particle-Assisted Organization of π-Conjugated Polymers into Highly Crystalline "Coffee Stains". *ACS Appl. Mater. Interfaces* **2017**, *9*, 34337−34348.
(9) Baranov, D.; Fiore, A.; Huis, M. V.; Giannini, C.; Falqui, A.; Lafont, U.; Zandbergen, H.; Zanella, M.; Cingolani, R.; Manna, L. Assembly of Colloidal Semiconductor Nanorods in Solution by Depletion Attraction. *Nano Lett.* **2010**, *10*, 743−749.
(10) Rupich, S. M.; Castro, F. C.; Irvine, W. T. M.; Talapin, D. V. Soft Epitaxy of Nanocrystal Superlattices. *Nat. Commun.* **2014**, *5*, No. 5045.
(11) Paik, T.; Diroll, B. T.; Kagan, C. R.; Murray, C. B. Binary and Ternary Superlattices Self-Assembled from Colloidal Nanodisks and Nanorods. *J. Am. Chem. Soc.* **2015**, *137*, 6662−6669.
(12) Kang, L.; Gibaud, T.; Dogic, Z.; Lubensky, T. C. Entropic Forces Stabilize Diverse Emergent Structures in Colloidal Membranes. *Soft Matter* **2016**, *12*, 386−401.
(13) Ye, X. C.; Zhu, C. H.; Ercius, P.; Raja, S. N.; He, B.; Jones, M. R.; Hauwiller, M. R.; Liu, Y.; Xu, T.; Alivisatos, A. P. Structural Diversity in Binary Superlattices Self-Assembled from Polymer-Grafted Nanocrystals. *Nat. Commun.* **2015**, *6*, No. 10052.
(14) Liang, Y. J.; Xie, Y.; Chen, D. X.; Guo, C. F.; Hou, S.; Wen, T.; Yang, F. Y.; Deng, K.; Wu, X. C.; Smalyukh, I. I.; Liu, Q. Symmetry Control of Nanorod Superlattice Driven by a Governing Force. *Nat. Commun.* **2017**, *8*, No. 1410.
(15) Man, X. K.; Doi, M. Ring to Mountain Transition in Deposition Pattern of Drying Droplets. *Phys. Rev. Lett.* **2016**, *116*, No. 066101.
(16) Chatterjee, S.; Kumar, M.; Murallidharan, J. S.; Bhardwaj, R. Evaporation of Initially Heated Sessile Droplets and the Resultant Dried Colloidal Deposits on Substrates Held at Ambient Temperature. *Langmuir* **2020**, *36*, 8407−8421.
(17) Zhao, C. Q.; Zhang, P. C.; Zhou, J. J.; Qi, S. H.; Yamauchi, Y.; Shi, R. R.; Fang, R. C.; Ishida, Y.; Wang, S. T.; Tomsia, A. P.; Liu, M. J.; Jiang, L. Layered Nanocomposites by Shear-Flow-Induced Alignment of Nanosheets. *Nature* **2020**, *580*, 210−215.
(18) Kim, H. S.; Lee, C. H.; Sudeep, P. K.; Emrick, T.; Crosby, A. J. Nanoparticle Stripes, Grids, and Ribbons Produced by Flow Coating. *Adv. Mater.* **2010**, *22*, 4600−4604.
(19) Lin, Y.; Balizan, E.; Lee, L. A.; Niu, Z.; Wang, Q. Self-Assembly of Rodlike Bio-nanoparticles in Capillary Tubes. *Angew. Chem.* **2010**, *122*, 880−884.
(20) Hong, S. W.; Byun, M.; Lin, Z. Q. Robust Self-Assembly of Highly Ordered Complex Structures by Controlled Evaporation of Confined Microfluids. *Angew. Chem. Int. Ed.* **2009**, *48*, 512−516.
(21) Perdana, J. A.; Fox, M. B.; Schutyser, M. A. I.; Boom, R. M. Single-Droplet Experimentation on Spray Drying: Evaporation of a Sessile Droplet. *Chem. Eng. Technol.* **2011**, *34*, 1151−1158.
(22) Wunsch, B. H.; Smith, J. T.; Gifford, S. M.; Wang, C.; Brink, M.; Bruce, R. L.; Austin, R. H.; Stolovitzky, G.; Astier, Y. Nanoscale Lateral Displacement Arrays for the Separation of Exosomes and Colloids down to 20 nm. *Nat. Nanotechnol.* **2016**, *11*, 936−940.
(23) Hu, H.; Larson, R. G. Analysis of the Effects of Marangoni Stresses on the Microflow in an Evaporating Sessile Droplet. *Langmuir* **2005**, *21*, 3972−3980.
(24) Du, L. N.; Sun, N. F.; Chen, Z. Y.; Li, Y. Y.; Liu, X. D.; Zhong, X. L.; Wu, X. C.; Xie, Y.; Liu, Q. Depletion-Mediated Uniform Deposition of Nanorods with Patterned, Multiplexed Assembly. *ACS Appl. Mater. Interfaces* **2020**, *12*, 49200−49209.
(25) Strizhak, P. A.; Volkov, R. S.; Misyura, S. Y.; Lezhnin, S. I.; Morozov, V. S. The Role of Convection in Gas and Liquid Phases at Droplet Evaporation. *Int. J. Therm. Sci.* **2018**, *134*, 421−439.
(26) Qi, W.; Li, J.; Weisensee, P. B. Evaporation of Sessile Water Droplets on Horizontal and Vertical Biphobic Patterned Surfaces. *Langmuir* **2019**, *35*, 17185−17192.
(27) Christy, J. R. E.; Hamamoto, Y.; Sefiane, K. Flow Transition within an Evaporating Binary Mixture Sessile Drop. *Phys. Rev. Lett.* **2011**, *106*, No. 205701.
(28) Liu, Q. K.; Senyuk, B.; Tang, J. W.; Lee, T.; Qian, J.; He, S. L.; Smalyukh, I. I. Plasmonic Complex Fluids of Nematiclike and Helicoidal Self-Assemblies of Gold Nanorods with a Negative Order Parameter. *Phys. Rev. Lett.* **2012**, *109*, No. 088301.
(29) Liu, Q. K.; Campbell, M. G.; Evans, J. S.; Smalyukh, I. I. Orientationally Ordered Colloidal Co-Dispersions of Gold Nanorods and Cellulose Nanocrystals. *Adv. Mater.* **2014**, *26*, 7178−7184.
(30) Kim, M. S.; Lee, S.; Koo, J. H.; Hong, J.; Chung, Y.; Son, K. J.; Koh, W. G.; Lee, T. Induced Transition of CdSe Nanoparticle Superstructures by Controlling the Internal Flow of Colloidal Solution. *ACS Appl. Mater. Interfaces* **2012**, *4*, 5162−5168.
(31) Sheetah, G. H.; Liu, Q. K.; Smalyukh, I. I. Self-assembly of Predesigned Optical Materials in Nematic Codispersions of Plasmonic Nanorods. *Opt. Lett.* **2016**, *41*, 4899−4902.
(32) Josyula, T.; Mahapatra, P. S.; Pattamatta, A. Insights into the Evolution of the Thermal Field in Evaporating Sessile Pure Water Drops. *Colloids Surf., A* **2020**, *611*, No. 125855.
(33) Xie, Y.; Guo, S. M.; Guo, C. F.; He, M.; Chen, D. X.; Ji, Y. L.; Chen, Z. Y.; Wu, X. C.; Liu, Q.; Xie, S. S. Controllable Two-Stage Droplet Evaporation Method and Its Nanoparticle Self-Assembly Mechanism. *Langmuir* **2013**, *29*, 6232−6241.
(34) Xie, Y.; Guo, S. M.; Ji, Yl.; Guo, C. F.; Liu, X. F.; Chen, Z. Y.; Wu, X. C.; Liu, Q. Self-Assembly of Gold Nanorods into Symmetric Superlattices Directed by OH-Terminated Hexa(ethylene glycol) Alkanethiol. *Langmuir* **2011**, *27*, 11394−11400.
(35) Hu, H.; Larson, R. G. Marangoni Effect Reverses Coffee-Ring Depositions. *J. Phys. Chem. B* **2006**, *110*, 7090−7094.
(36) Ungureanu, C.; Rayavarapu, R. G.; Manohar, S.; Leeuwen, T. V. Discrete Dipole Approximation Simulations of Gold Nanorod Optical Properties: Choice of Input Parameters and Comparison with Experiment. *J. Appl. Phys.* **2009**, *105*, 1870−1871.
(37) Hanske, C.; Hill, E. H.; Vila-Liarte, D.; Gonzalez-Rubio, G.; Matricardi, C.; Mihi, A.; Liz-Marzán, L. M. Solvent-Assisted Self-Assembly of Gold Nanorods into Hierarchically Organized Plasmonic Mesostructures. *ACS Appl. Mater. Interfaces* **2019**, *11*, 11763−11771.
(38) Xie, Y.; Li, Y. Y.; Wei, G. Q.; Liu, Q. K.; Mundoor, H.; Chen, Z. Y.; Smalyukh, I. I. Liquid Crystal Self-Assembly of Upconversion Nanorods Enriched by Depletion Forces for Mesostructured Material Preparation. *Nanoscale* **2018**, *10*, 4218−4227.
(39) Liu, Q. K.; Cui, Y. X.; Gardner, D.; Li, X.; He, S. L.; Smalyukh, I. I. Self-Alignment of Plasmonic Gold Nanorods in Reconfigurable Anisotropic Fluids for Tunable Bulk Metamaterial Applications. *Nano Lett.* **2010**, *10*, 1347−1353.
(40) Cazabat, A. M.; Heslot, F.; Troian, S. M.; Carles, P. Fingering Instability of Thin Spreading Films Driven by Temperature Gradients. *Nature* **1990**, *346*, 824−826.
(41) Buffone, C.; Sefiane, K. Investigation of Thermocapillary Convective Patterns and Their Role in the Enhancement of Evaporation from Pores. *Int. J. Multiphase Flow* **2004**, *30*, 1071−1091.
(42) Wang, H.; Murthy, J. Y.; Garimella, S. V. Transport from a Volatile Meniscus inside an Open Microtube. *Int. J. Heat Mass Transfer* **2008**, *51*, 3007−3017.
(43) Bennacer, R.; Sefiane, K.; El-Ganaoui, M.; Buffone, C. Numerical Investigation of the Role of Non-Uniform Evaporation Rate in Initiating Marangoni Convection in Capillary Tubes. *Int. J. Numer. Methods Heat Fluid Flow* **2004**, *14*, 879−892.
(44) Deng, J.; Liang, W. L.; Fang, J. Y. Liquid Crystal Droplet-Embedded Biopolymer Hydrogel Sheets for Biosensor Applications. *ACS Appl. Mater. Interfaces* **2016**, *8*, 3928−3932.
(45) ten Wolde, P. R.; Frenkel, D. Enhancement of Protein Crystal Nucleation by Critical Density Fluctuations. *Science* **1997**, *277*, 1975−1978.

https://doi.org/10.1021/acsami.1c12594
ACS Appl. Mater. Interfaces 2021, 13, 53143−53154

(46) Anderson, V. J.; Lekkerkerker, H. N. W. Insights into Phase Transition Kinetics from Colloid Science. *Nature* **2002**, *416*, 811−815.
(47) de Gennes, P. G. An Analogy between Superconductors and Smectics A. *Solid State Commun.* **1972**, *10*, 753−756.
(48) Gibaud, T.; Barry, E.; Zakhary, M. J.; Henglin, M.; Ward, A.; Yang, Y. S.; Berciu, C.; Oldenbourg, R.; Hagan, M. F.; Nicastro, D.; Meyer, R. B.; Dogic, Z. Reconfigurable Self-Assembly through Chiral Control of Interfacial Tension. *Nature* **2012**, *481*, 348−351.
(49) Nayani, K.; Chang, R.; Fu, J. X.; Ellis, P. W.; Fernandez-Nieves, A.; Park, J. O.; Srinivasarao, M. Spontaneous Emergence of Chirality in Achiral Lyotropic Chromonic Liquid Crystals Confined to Cylinders. *Nat. Commun.* **2015**, *6*, No. 8067.
(50) Zakhary, M. J.; Gibaud, T.; Kaplan, C. N.; Barry, E.; Oldenbourg, R.; Meyer, R. B.; Dogic, Z. Imprintable Membranes from Incomplete Chiral Coalescence. *Nat. Commun.* **2014**, *5*, No. 3063.
(51) Xie, Y.; Liang, Y. J.; Chen, D. X.; Wu, X. C.; Dai, L. R.; Liu, Q. Vortical Superlattices in a Gold Nanorods' Self-Assembled Monolayer. *Nanoscale* **2014**, *6*, 3064−3068.
(52) Sung, B.; de la Cotte, A.; Grelet, E. Chirality-Controlled Crystallization via Screw Dislocations. *Nat. Commun.* **2018**, *9*, No. 1405.
(53) Xie, Y.; Jia, Y. F.; Liang, Y. J.; Guo, S. M.; Ji, Y. L.; Wu, X. C.; Chen, Z. Y.; Liu, Q. Real-Time Observations on Crystallization of Gold Nanorods into Spiral or Lamellar Superlattices. *Chem. Commun.* **2012**, *48*, 2128−2130.
(54) Lee, H.; Sunkara, V.; Cho, Y. K.; Jeong, J. Effects of Poly(Ethylene Glycol) on the Wetting Behavior and Director Configuration of Lyotropic Chromonic Liquid Crystals Confined in Cylinders. *Soft Matter* **2019**, *15*, 6127−6133.
(55) Guerrero-Martínez, A.; Perez-Juste, J.; Carbo-Argibay, E.; Tardajos, G.; Liz-Marzán, L. M. Gemini-Surfactant-Directed Self-Assembly of Monodisperse Gold Nanorods into Standing Superlattices. *Angew. Chem.* **2009**, *121*, 9648−9652.
(56) Scheinfein, M. R.; Unguris, J.; Celotta, R. J.; Pierce, D. T. Influence of the Surface on Magnetic Domain-Wall Microstructure. *Phys. Rev. Lett.* **1989**, *63*, 668.
(57) Seč, D.; Porenta, T.; Ravnik, M.; Žumer, S. Geometrical Frustration of Chiral Ordering in Cholesteric Droplets. *Soft Matter* **2012**, *8*, 11982−11988.

https://doi.org/10.1021/acsami.1c12594
ACS Appl. Mater. Interfaces 2021, 13, 53143−53154